PNAS RESEARCH ARTICLE | ENGINEERING

Folding a single high-genus surface into a repertoire of metamaterial functionalities

Xiangxin Dang[a], Stefano Gonella[b,1], and Glaucio H. Paulino[a,c,1]

Affiliations are included on p. 10.

Edited by Yonggang Huang, Northwestern University—Evanston, Glencoe, IL; received July 3, 2024; accepted September 12, 2024

The concepts of origami and kirigami have often been presented separately. Here, we put forth a synergistic approach—the folded kirigami—in which kirigami assemblies are complemented by means of folding, typical of origami patterns. Besides the emerging patterns themselves, the synergistic approach also leads to topological mechanical metamaterials. While kirigami metamaterials have been fabricated by various methods, such as 3D printing, cutting, casting, and assemblage of building blocks, the "folded kirigami" claim their distinctive properties from the universal folding protocols. For a target kirigami pattern, we design an extended high-genus pattern with appropriate sets of creases and cuts, and proceed to fold it sequentially to yield the cellular structure of a 2D lattice endowed with finite out-of-plane thickness. The strategy combines two features that are generally mutually exclusive in canonical methods: fabrication involving a single piece of material and realization of nearly ideal intercell hinges. We test the approach against a diverse portfolio of triangular and quadrilateral kirigami configurations. We demonstrate a plethora of emerging metamaterial functionalities, including topological phase-switching reconfigurability between polarized and nonpolarized states in kagome kirigami, and availability of nonreciprocal mechanical response in square-rhombus kirigami.

kirigami | origami | topological mechanics | polarization | reciprocity

Significance

Metamaterials with sophisticated mechanical behavior can be realized based upon two restrictive, but synergistic, operations: 1) cutting, and 2) folding. In general, kirigami structures obtained via canonical manufacturing, e.g., 3D-printing, cutting or casting, suffer from a detrimental competition between in-plane stiffness and out-of-plane strength, which hinders their response. Different from mainstream approaches, our strategy allows realizing kirigami of arbitrary geometric complexity relying exclusively on sequences of folding operations performed on a single sheet. These "folded kirigami" shine for the diversity, precision, and reliability of their mechanical performance, featuring metamaterial functionalities, such as topological polarization and nonreciprocity. Our "folded kirigami" prototypes display extreme tunability, thanks to their nearly ideal hinges allowing seamless switching between different configurations.

Mechanical metamaterials are structural materials that derive their distinctive mechanical properties from the geometry and connectivity of their internal architecture rather than from the material composition of its constituent elements (1, 2). They are known to display an array of unconventional mechanical properties typically unattainable in conventional continua, such as auxeticity (3, 4), negative effective elastic moduli and density (5–7) and extreme reconfigurability under loading (8, 9). The key properties of metamaterials are controlled by the geometry and real-space topology of their geometric layouts, which, in the case of periodic metamaterials, boils down to the shapes of their unit cells. Recently, the intersection of topological mechanics and metamaterial design has led to the discovery of new classes of mechanical metamaterials whose response is attributable to the topology of their phonon band structure—the so-called k-space topology. An example of mechanical systems whose properties are heavily dictated by their k-space topology is topological Maxwell lattices, a subset of Maxwell lattices which, as a result of broken symmetries in their unit cells, have the ability to be topologically polarized (10–17). This property, which manifests as the ability to focus floppy modes and stress-bearing modes on opposite edges of a finite domain, is controlled by the k-space topology of the lattice band structure and is therefore protected against perturbations of the local geometric features of the edges, provided that the topological properties of the bulk remain unchanged. When a floppy edge is loaded by a point force, its softness allows the onset of localized deformation. In contrast, a similar load applied to the rigid edge necessarily results in rigid body motion of the entire domain.

While these conditions are formally predicted for ideal lattices, in which the bonds are connected by perfect hinges, a diluted signature is also observed in structural lattices, e.g., lattices fabricated via additive or subtractive manufacturing techniques, where the ideal hinges are replaced by elastic ligaments with finite bending stiffness (18–22). One can refer to such systems as topological kagome metamaterials. Strictly speaking, the polarization, as defined above, and its topological character are germane to the linear elastic regime of deformation. Nevertheless, it has been shown that their signatures carry over into the nonlinear finite-deformation regime, where their signatures are actually magnified. Here, the polarization manifests as a profound asymmetry in the deformation patterns observed on the edges, with the soft edge exhibiting large localized deformation

The authors declare no competing interest.

This article is a PNAS Direct Submission.

[1]To whom correspondence may be addressed. Email: sgonella@umn.edu or gpaulino@princeton.edu.

This article contains supporting information online at https://www.pnas.org/lookup/suppl/doi:10.1073/pnas.2413370121/-/DCSupplemental.

Published November 8, 2024.

akin to the response to an indenter, and the stiff edge activating a small deformation that leaks deep into the bulk (19, 23–25). Practically, dealing with soft mechanical metamaterials that are loaded statically, a geometrical nonlinear response is activated de facto in most experimental characterizations where a naked-eye inspection of the deformation is sought.

Kirigami (cutting paper) is an emerging method to program large deformations of 2D surfaces by perforating slits and dividing the surfaces into interconnected panels (26). The 2D surfaces with slits, or called kirigami surfaces, are generally flat, but can also be curved with zero Gaussian curvature [e.g., cylindrical surface (27)] or intrinsically with nonzero Gaussian curvature [e.g., spherical surface (28)]. The following two factors play vital roles in defining deformations of kirigami surfaces: first, the distributions of slits; second, the ratio of surface thickness to hinge width (residual size at intersecting area of slits). The distributions of slits generally dictate global deformations of kirigami surfaces, which can be designed by geometrical analysis with the assumption of ideal hinges (or generally joints) (29, 30). In this case, the kirigami surfaces are deemed mechanisms in which the stiffness of joints is much smaller than that of the panels. However, if the panels are integrated with compliant hinges of small thickness-to-width ratio, the global shape changes of kirigami surfaces are largely affected by unstable local deformations (e.g., nondirectional rotation and unstable buckling) at the joints (9). Buckling-induced instability can be utilized to trigger desired deformation modes of thin and soft kirigami surfaces (31, 32), but is undesirable for thick kirigami mechanisms aimed for precise control of local deformations (33–35). Current approaches to fabricating kirigami mechanisms of finite thickness, which is not as straightforward as cutting thin sheets, mainly include 3D printing (35), cutting thick plates (29), casting with molds (34), and assembling building blocks (33). By the former three approaches, one generally uses materials with high toughness (say, thermoplastic polyurethane for 3D printing, rubber for cutting or casting), and obtains an integral piece of plate with the panels connected by compliant hinges of residual materials. It is worth noting that one has to seek balance between stiffness and strength of the residual materials—adequate residual materials contribute to high strength to avoid damage of the surfaces, but on the other hand, they cause high stiffness and induce large restoring forces that may hinder large deformations. By the assembling approach, one can fabricate (e.g., 3D print or fold with paper) each panel separately and connect them with tapes. In this way, one obtains a mechanism with significantly low rotational stiffness at the hinges. However, the out-of-plane stiffness of tapes is also extremely low, making the whole system too soft to maintain its shape without a supporting surface, and therefore the application scenarios are limited.

Addressing simultaneously the individual limitations of the kirigami and of the multipart assembly methods, in an effort to design metamaterials with the proper balance of strength and stiffness within a unitary design framework, in this work, we put forth an alternative strategy to realize 2D kirigami via pure folding of a single high-genus sheet. To this end, we introduce a two-step fabrication protocol, in which we first prescribe creases and slits (holes), turning the sheet into a high-genus topological object, and subsequently we fold it into finite-thickness 2D kirigami mechanisms with nearly ideal hinges. We call the kirigami mechanisms resulting from this process "folded kirigami", to emphasize the fact that they have the geometric appearance of conventional kirigami patterns (e.g., the kagome and the rotating-square patterns), but they are folded from single crease-and-slit-endowed sheets according to rational folding sequences dictated by the desired kirigami patterns. In summary, two key features characterize a "folded kirigami:" 1) in terms of geometry, the fact that it is obtained from a single piece of paper; 2) in terms of mechanics, that its hinges can be essentially regarded as creases with low rotational stiffness.

In the remainder of the paper, we explore this paradigm against a variety of kirigami patterns, detailing for each the required geometric features of the primitive high-genus sheet and the steps of the folding process. The presented portfolio includes two patterns that stand out for their geometric and mechanical complexity and have been put forth in recent years as prototypical systems in topological mechanics: a topologically polarized stretched and twisted kagome (Maxwell) lattice, which is expected to feature a floppy-rigid edge dichotomy (36), and an undercoordinated quadrilateral lattice that has been shown to display nonreciprocal response under static loads (37). For these, we perform mechanical tests to illustrate experimentally how their unique mechanical properties, which were previously demonstrated using conventionally fabricated (3D-printed, cut or cast) prototypes, can be observed with remarkable high-fidelity and comparable accuracy also in the "folded kirigami" specimens—a testament to the near-ideal conditions of the folded hinges.

Results

Regular Kagome Pattern. The classical triangular kirigami pattern—widely known as the kagome pattern—is composed of equilateral triangles enclosing hexagonal holes. The planar kagome mechanism correspondingly has hinged equilateral-triangular prisms as its building blocks. To show how to make a planar kagome mechanism from one piece of paper, we start by folding an equilateral-triangular patch to a prism with hinges aligning its lateral edges (Fig. 1*A*). The key idea is to fold the rectangular wings and make the included right-triangular flaps coincide, such that free hinges are created between the coinciding flaps and the main prism. The hinges are perpendicular to the base of the prism, because each of them is perpendicular to two edges of the base. Upon application of threefold rotational symmetry, the folding process involves a single degree of freedom (DoF). Consequently, we have three dependent dihedral angles: the angle θ between the base and a wing, the angle ξ between a wing and a flap, and the angle φ between two flaps. Using spherical trigonometry, we obtain relationships between θ, ξ, and φ as follows (*SI Appendix*, section 1 and Fig. S1):

$$\varphi = 2\theta - \pi \qquad [1]$$

and

$$\xi = \pi - \arccos\left(\tan\frac{\alpha}{2}\tan\frac{\gamma}{2}\right) + \arccos\left(-\frac{\sin\alpha\cos\theta}{\sin\gamma}\right), \qquad [2]$$

in which α is the interior angle of the base triangle, i.e., $\alpha = \pi/3$; and γ is the included angle between intersecting edges of two wings, expressed by

$$\gamma = -2\arcsin\left(\cos\frac{\alpha}{2}\cos\theta\right). \qquad [3]$$

All the three dihedral angles are initially equal to π. We define the folding angle $\rho = \pi - \theta$ as an independent variable, and plot curves of φ and ξ throughout the folding process (Fig. 1*B*). When ρ increases from 0 to $\pi/2$ (or equivalently, θ decreases from π to $\pi/2$), the folding finally stops at $\varphi = \gamma = 0$, which indicates

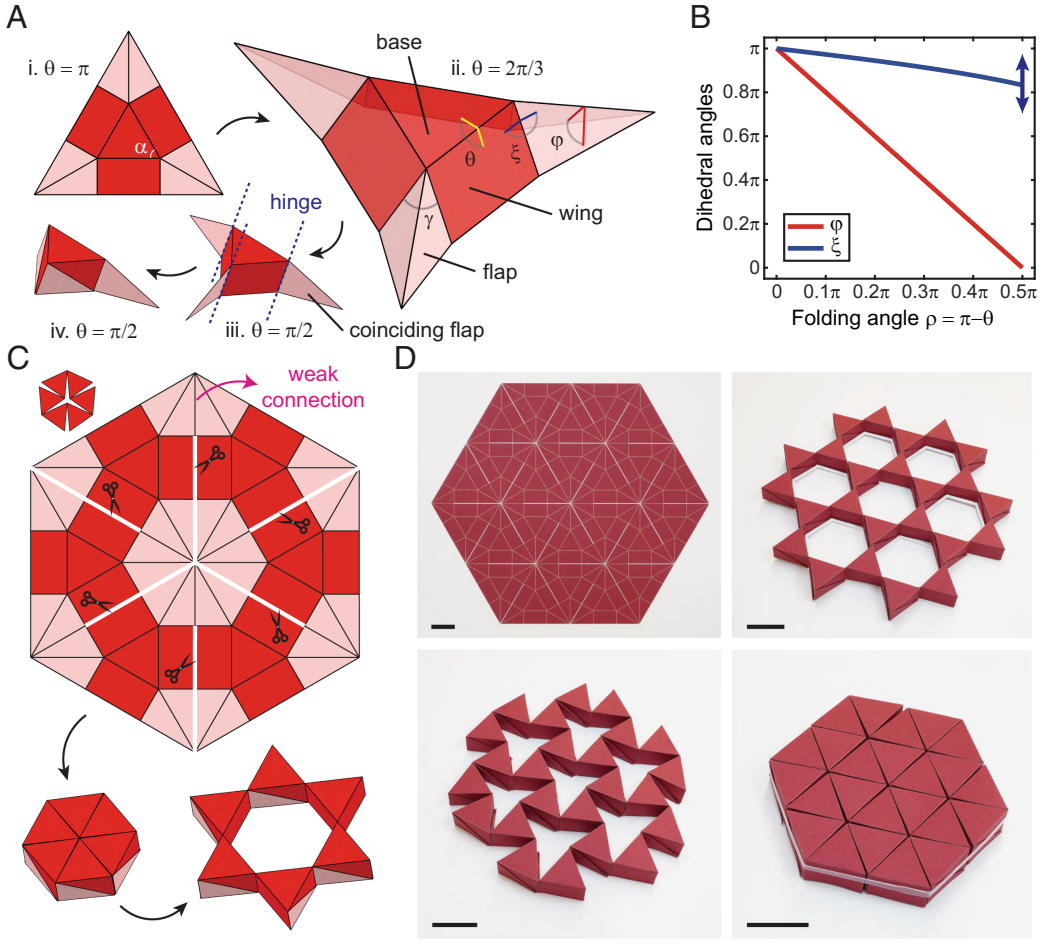

Fig. 1. "Folded kirigami" from the regular kagome pattern. (*A*) Crease pattern for a single equilateral-triangular prism and its folding sequence. (*B*) Curves of dihedral angles φ and ξ versus the folding angle $\pi - \theta$. (*C*) Crease-slit pattern and its folded configurations for the single-loop kagome mechanism. (*D*) Paper sheet with perforated cuts and engraved creases for the multiloop kagome mechanism (*Top Left*) and its folded configurations. (Scale bars, 3 cm.)

the flaps (or equivalently, their edges) coincide and constitute the lateral edges of a prism. The coinciding flaps can freely rotate around the lateral edges, reflected by the two arrows at the end of the curve of ξ. In other words, hinges are created along the three lateral edges. By attaching some of the flaps onto the prism, i.e., fixing $\xi = 0$ or 2π, we can suppress the rotation at the corresponding hinges on demand (Fig. 1 *A*, *iv*).

To fold a kagome mechanism from one piece of paper, we propose a crease-slit pattern composed of creased equilateral-triangular patches (Fig. 1*C*). These creased patches are weakly connected only at common edges of the flaps that are supposed to form hinges. For each weak connection, four flaps coincide by folding and are attached onto a prism. As a result, we create hinges perpendicular to the base triangles, allowing free in-plane rotation between the prisms. To validate the proposed folding approach, we fabricate a paper sheet with perforated cuts and engraved creases (Fig. 1 *D, Top Left*). After folding the single piece of paper and gluing the flaps onto the prisms, we obtain the "folded kirigami" that can be fully deployed to have regular hexagonal holes (Fig. 1 *D, Top Right*) and fully retracted to a void-free configuration (Fig. 1 *D, Bottom Right*) via a global soft mode known as Guest-Hutchinson (GH) mode (38). In practice, it is not easy to drive the kagome "folded kirigami" deforming via the GH mode because of its multi-DoF nature. A neutral-equilibrium state near the GH mode is shown in Fig. 1*D* (*Bottom Left*). We refer to Movie S1 for the simulated deployment and retraction of the kagome "folded kirigami" via its GH mode.

Irregular Kagome Pattern. Our folding approach creates hinges by common edges of the coinciding flaps. The weak connections of the adjacent flaps essentially guide the shape-shifting (folding and attaching) process. In other words, by folding along the creases, we align the common edges automatically, which is efficient and accurate compared to making the prisms separately and then assembling them together. This principle is universal and can be easily generalized to make diverse 2D mechanisms. We exemplify such universality with the irregular kagome pattern obtained by repeating equilateral triangles and scalene triangles, which is of special interest by virtue of its applications in topological metamaterials (36, 39). Fig. 2*A* shows a single loop of the irregular kagome pattern, with its GH-mode deformation controlled by the twist angle θ. Retracting the single loop to $\theta = 0$, we can obtain a compact configuration, but the enclosed area cannot be eliminated to zero (Fig. 2 *A*, *Bottom*), which leaves V-shaped gaps between some triangles. This is different from the regular kagome pattern, which has a complete compact configuration with no voids. Fig. 2*B* shows how to design the crease pattern and to create a hinge between two triangles with a V-shaped gap: (*i*) extract the two triangles from the kagome pattern; (*ii*) add rectangular wings with a unified width h; (*iii*) add right-triangular flaps at each vertex; (*iv*) truncate the flaps to a unified residual side length s; (*v*) connect the two flaps where the hinge is supposed to be created; (*vi*) fill the V-shaped gap by extending edges of rectangular wings, finalizing the crease pattern; (*vii*) fold and attach the flaps onto the

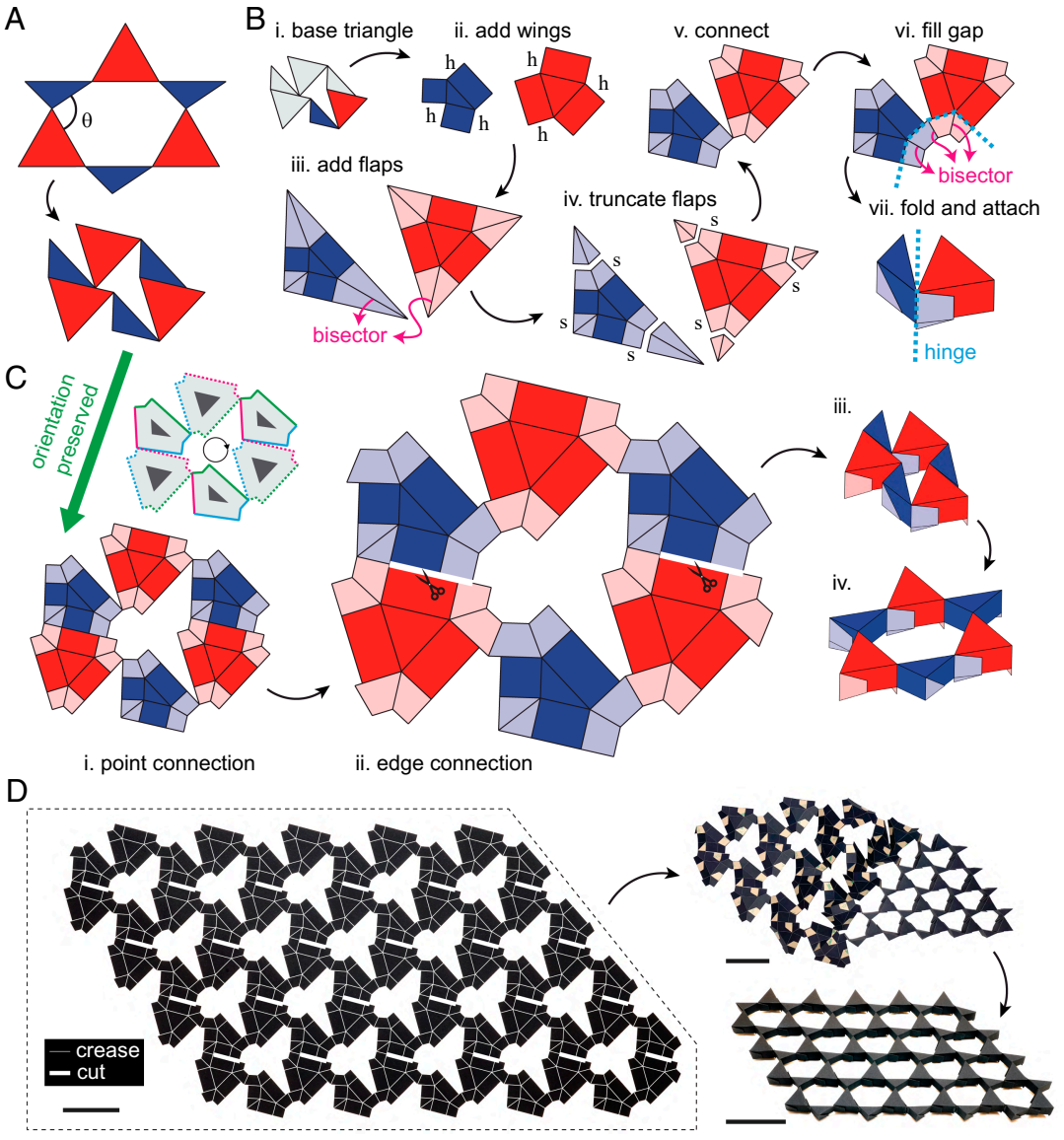

Fig. 2. Irregular kagome pattern and the "folded kirigami". (*A*) Single reconfigurable loop of the irregular kagome pattern. (*B*) Step-by-step description for generating the crease pattern that is folded to two triangular prisms with a hinge. (*C*) Point-connected layout (*i*), crease-slit pattern (*ii*), and its folded configurations (*iii* and *iv*) for the irregular kagome "folded kirigami" with a single loop. (*D*) Paper sheet with perforated cuts and engraved creases for the irregular kagome "folded kirigami" with multiple loops (*Left*) and its partially folded (*Top Right*) and fully folded (*Bottom Right*) configurations. (Scale bars, 5 cm.)

prisms, thus obtaining the hinge. Throughout the procedure above, we have preserved the orientations of the base triangles. In short, for the given base triangles, we determine the crease pattern by two parameters h and s, which can be specified on demand. The parameter h is also the height (or thickness) of the folded 2D mechanism. The key point that makes the procedure effective is that we essentially create three bisectors, guiding the four lateral edges to coincide and to form the desired hinge (Fig. 2 *B*, *vi* and *vii*).

The patches with truncated flaps can interconnect to a closed loop with their base triangles oriented in the same way as in the original kagome pattern (GH mode), because the hole is essentially enclosed by full boundaries of the two repeating creased patches (Fig. 2 *C*, *Top Left*). This fact allows folding an irregular kagome mechanism from one piece of paper forsaking the need to adjust the orientations of the base triangles. To finalize the crease pattern, we fill the V-shaped gap at each vertex by extending edges of rectangular wings (Fig. 2 *C*, *ii*). Then we can fold from the pattern and attach the coinciding flaps to prisms, creating the 2D mechanism with multiple hinges (Fig. 2 *C*, *iii* and *iv*). We refer to *SI Appendix*, section 2 and Fig. S2 for detailed formulations and illustrations of the crease-slit patterns. By replicating the single pattern, we can obtain the crease-slit patterns for the "folded kirigami" with multiple loops. For example, we fabricate a paper sheet and fold it (and attached the flaps) to an irregular kagome mechanism with 5-by-4 holes (Fig. 2*D*). The paper sheet also has 5-by-4 holes and therefore is as high-genus as the "folded kirigami" from the viewpoint of topology. We note that the crease-slit pattern of a regular kagome kirigami (e.g., Fig. 1 *D*, *Top Left*) is also high-genus, consistent with the folded mechanism (e.g., Fig. 1 *D*, *Top Right*). The discrepancy of the two repeating triangles gives rise to expanding of slits to holes from regular to irregular kagome patterns (Movie S2). Finally, the intermediate half-folded state in Fig. 2*D* shows how having weak connections between flaps promotes the folding process—the folding can be

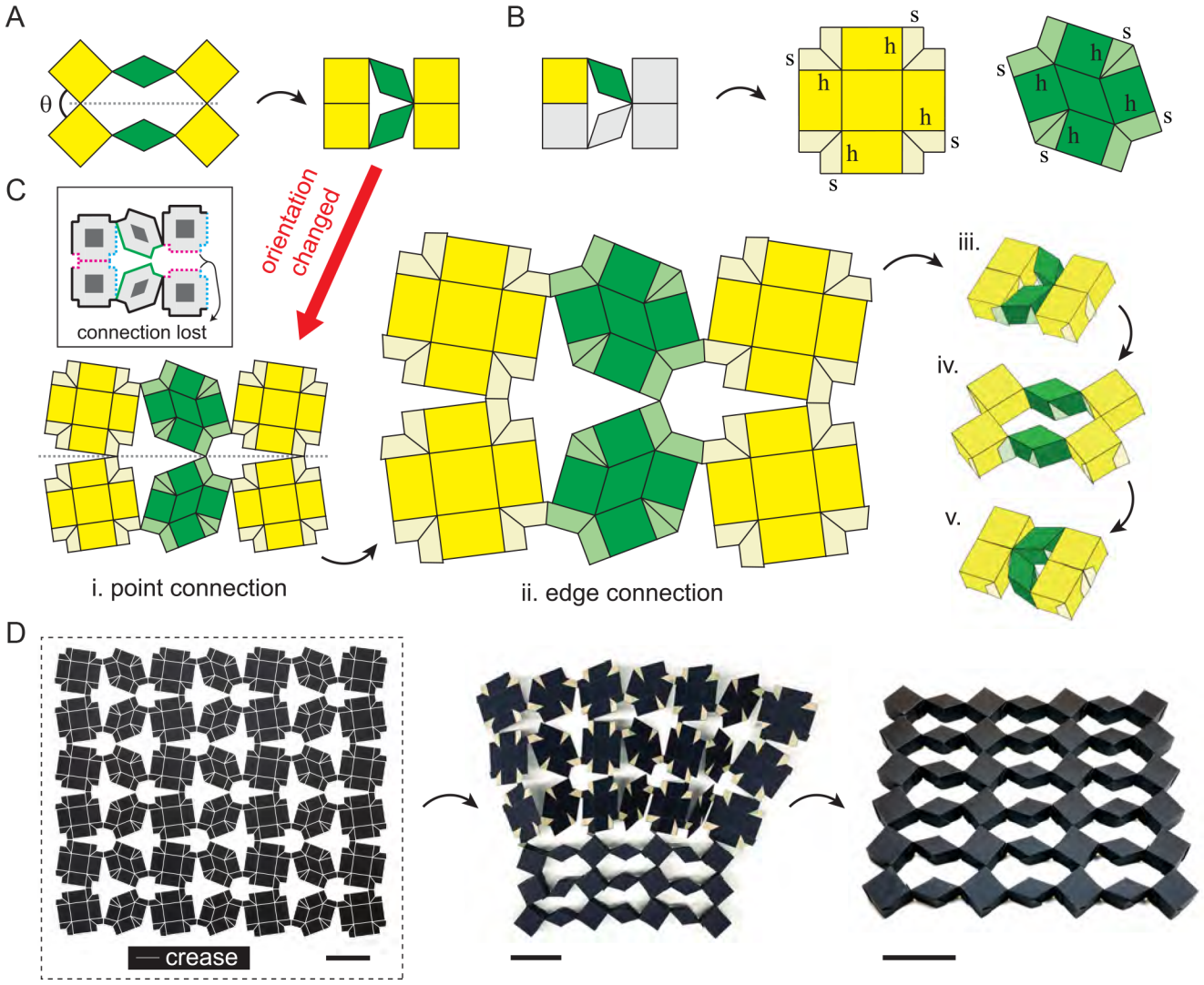

Fig. 3. Square-rhombus pattern and the "folded kirigami". (*A*) Single reconfigurable loop of the square-rhombus pattern. (*B*) Crease patterns of the extracted square and rhombus. (*C*) Point-connected layout with adjusted orientation (*i*), crease-slit pattern (*ii*), and its folded configurations (*iii*–*v*) for the square-rhombus "folded kirigami" with a single loop. (*D*) Paper sheet with perforated cuts and engraved creases for the square-rhombus "folded kirigami" with multiple loops (*Left*) and its partially folded (*Middle*) and fully folded (*Right*) configurations. (Scale bars, 5 cm.)

done sequentially from cell to cell while the system preserves the prescribed connections.

Quadrilateral Pattern. Our proposed folding approach is applicable beyond triangles and can be generalized to convex polygonal bases, because the flaps (that form a hinge) are built based on local information, i.e., one vertex and two edges for each of the two adjacent polygonal bases connected by the hinge. Here, we invoke the folded rotating-square configuration in *SI Appendix*, Fig. S3 and Movie S3 as a proxy for a broader class of quadrilateral kirigami systems. Moreover, we consider a square-rhombus kirigami pattern that is different from either the kagome or the rotating-square patterns, in the sense that the orientations of base polygons have to be properly adjusted when designing the crease-slit pattern for the "folded kirigami". This kirigami pattern has been explored to illustrate nonreciprocity in mechanical metamaterials (37), using a configuration featuring a unit composed of four squares and two rhombi that are mirror-symmetric about a horizontal line (Fig. 3 *A*, *Left*). The kirigami unit is reconfigurable by changing the angle θ between adjacent edges of squares across the mirror line, and is compact for $\theta = 0$ (Fig. 3 *A*, *Right*). To design the crease-slit pattern, first, we extract a square and a rhombus from the kirigami unit and construct the creased patches by adding wings and truncated flaps at each of their vertices with height h and residual side length s (Fig. 3*B*). However, when we try to connect the creased patches following the same orientation of the compact kirigami unit (Fig. 3 *A*, *Right*), we lose one connection on the right end (Fig. 3 *C*, *Top Left*). This fact indicates that connections in the original kirigami do not guarantee connections of the creased patches—we may lose some connections when building the crease-slit pattern out of multiple creased patches. This issue can be solved in two different ways. The first way is simply by abandoning these connections in the crease-slit pattern and still attaching the flaps after folding. This way, however, is not recommended because it makes the shape shifting (to 2D mechanism) less guided. The second way, which is more elegant, is by adjusting the orientation of the creased patches and rebuilding the point connection (Fig. 3 *C*, *i*). For our current approach, we performed the orientation adjustment by trial and error. Once the full point connection is obtained, the following step are to build the edge connections by filling the V-shaped gaps between flaps for hinges (Fig. 3

C, *ii*), and to fold the crease-slit pattern into a 2D mechanism (Fig. 3 *C*, *iii–v*). In analogy to the irregular kagome pattern, we fabricate a high-genus sheet and fold it (and attached the flaps) to obtain the square-rhombus "folded kirigami" with 5-by-3 holes (Fig. 3*D*). Again, the intermediate half-folded state (Fig. 3 *D*, *Middle*) shows that the weak connections between flaps contribute to the sequential folding. In addition to the low-cost (using origami paper and glue/tapes) and easy-to-do (folding and attaching) fabrication process, we show that the "folded kirigami" (Figs. 2 *D*, *Bottom Right* and 3 *D*, *Right*) also inherit the unique mechanical functionalities from the original kirigami patterns (irregular kagome kirigami and square-rhombus kirigami).

Tunable Topologically Polarized Mechanics of Kagome "Folded Kirigami". In the previous section, we have demonstrated the versatility of the proposed technique by showing that a portfolio of configurations are achievable by slightly tailoring a shared folding procedure. We now show that the 2D cellular metamaterials obtained by folding do not only stand out for the outstanding accuracy of their geometric details but also feature precise and reliable mechanical properties. These properties are on par with solid prototypes fabricated using additive or subtractive manufacturing and, in some respects, even superior in terms of versatility and tunability. The experiments described in this and the next section attest to these attributes by demonstrating how the prototypes display a mechanical response under loading that matches precisely theoretical predictions and experimental results obtained on cast or 3D-printed specimens. To this end, we consider two lattices that are expected to display an asymmetric mechanical response between their edges (due to topological polarization and nonreciprocity, respectively) and we extract the signature of such asymmetry from laboratory testing.

The first case regards the kagome "folded kirigami" in Fig. 2*D*, which is a prototypical example of a configuration featuring topologically protected polarization, whereby floppy edge modes localize on one edge, deemed "floppy edge," while stress-bearing modes focus on the opposite edge that behaves rigidly. In statics, the phenomenon manifests as a behavioral edge asymmetry in which the floppy edge experiences large localized deformation, while the opposite edge, under the same load, responds as a stiff boundary. The topological protection proceeds from the fact that the polarization, while manifesting as an edge effect, is an intrinsic property of the bulk, and is therefore preserved as long as the topology of the bulk is not altered. The specific configuration in Fig. 2*D* was discussed by Rocklin et al. in their study on transformable mechanical metamaterials (36). Using phase diagrams, they showed that, by sweeping the twist angle—which corresponds to subjecting the lattice to a GH mode—the lattice can be transformed back and forth between a polarized and a nonpolarized state. As shown in the *Insets* of Fig. 4 *B* and *C*, the two configurations of different twist angles θ capture a polarized (with horizontal parallel edges) and a nonpolarized state (with inclined parallel edges), respectively.

Our goal is to use a single "folded kirigami" prototype to switch between two configurations characterized by vastly different twist angles and verify experimentally the resulting gain and loss of polarization. To this end, we need to configure the lattice in two states and, for each state, subject the prototype to two sets of static compression tests, applying a load on opposite edges and comparing the local displacement of the loaded edges. These setup requirements introduce a practical challenge. As stated above, the reconfiguration involves the application of a GH mode, which is a global soft mode of the bulk. In practice, it is virtually impossible to properly establish a GH mode via simple traction loads applied at the boundaries. To achieve that, one needs to prescribe a displacement path to all the edge cells of the lattice, which would in turn enforce the proper twist pattern to the cells of the bulk. This strategy was adopted in ref. 24, where, for a kagome sample mounted on a substrate, the edges were pinned to moving slits which could slide relatively to the substrate deforming the lattice according to a desired pattern. For our problem, we adapt a similar approach to the "folded kirigami" prototype. We design and fabricate holding frames featuring arrays of triangular protruding elements to which we can anchor the edge cells of the "folded kirigami" prototype, as shown in Fig. 4*A* and *SI Appendix*, Fig. S4 *A* and *B*. Here, we take advantage of the hollow nature of the paper cells, which allows constraining them by simply inserting prismatically the solid triangles of the frames. We build two interchangeable frames, shown in Fig. 4 *B* and *C*, one for the polarized and one for the nonpolarized case, and we switch between them through the testing.

The compression tests are conducted using a materials testing machine, shown in Fig. 4*A*, operating in displacement control. We probe the edge of the specimen with a loading tip, imposing a prescribed point displacement while measuring the applied force with a load cell. We quasi-statically ramp the imposed displacement from 0 to 5 mm, a range expected to fall within the linear elastic regime of the metamaterial. A setup detail worth of notice regards the loading tip used in our experiments. In tests devoted to assess polarization, it is crucial to discriminate between the deformation due to the polarization, which does not depend on the specific geometric features of the edge, from the trivial one (that any edge naturally exhibits), which is instead dictated by the edge morphology. Since the trivial deformation is typically dominated by rotations of the protruding edge triangles, an effective way to filter out this component of the response is by imposing the load in a way that prevents, as much as possible, such rotations. This goal can be achieved by endowing the loading tips with V-notches that rigidly engage the triangular blocks, effectively forcing them to translate without rotations (24, 40). Here, we adopt this approach, with an important setup modification: Since we are testing two configurations (polarized and nonpolarized) and two edges (A and B) per configuration, for a total of four distinct edge profiles, we custom-fabricate four tips with shapes tailored to those profiles (*SI Appendix*, Fig. S4 *A* and *B*).

Armed with these considerations, we can inspect and interpret the results of the tests. Let us begin with the test of the polarized configuration, shown in Fig. 4*D*. The *Left* panel refers to the loading of edge A (expected to be floppy) and the *Right* panel to the loading of edge B (expected to be rigid). In Fig. 4*E*, we report the force–displacement curves measured during the test. For both edges, the behavior is mostly linear, albeit with a softening region appearing in the 1 to 2 mm displacement interval in the loading history of edge B, arguably due to some settlement of the paper connections occurring around that force value. The macroscopic difference in slope between the curves provides a quantification of the stiffness gap between the edges due to polarization, confirming that edge A is indeed floppy. For each case, the *Inset* in Fig. 4*D* shows a close-up detail of the loaded edge, showing the deformed cells against the undeformed pattern (black solid lines): Under the same load of 0.37 N, the displacement $u_A = 5$ mm for edge A is significantly larger than $u_B = 1$ mm for edge B. This visual signature of the gap in compliance further confirms the floppy nature of edge A and the lattice polarization. We repeat the process for the other configuration, as shown in Fig. 4 *F* and *G*. Here, in sharp contrast

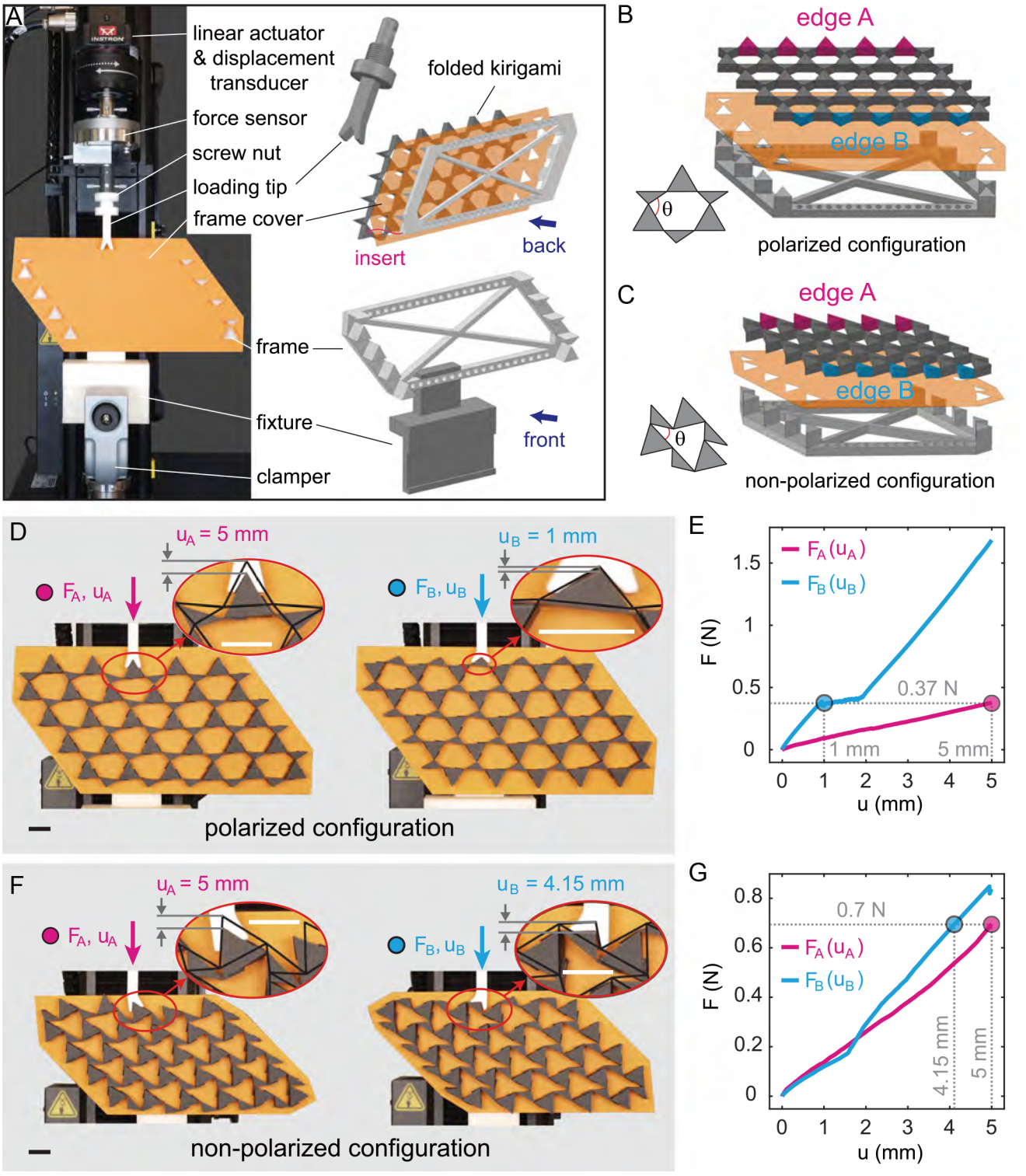

Fig. 4. Experimental validation of tunable topological polarization in kagome "folded kirigami". (*A*) Setup for the compression tests. (*B*) Polarized and (*C*) nonpolarized configurations of the "folded kirigami" shown with the corresponding frame and cover. (*D*) Floppy and rigid edge deformations of the polarized configuration with *Insets* highlighting the neighborhood of the loading point. (Scale bars, 2 cm.) (*E*) Force–displacement curves for loads applied at edges A (floppy) and B (rigid). (*F*) Edge deformations of the nonpolarized configuration with *Insets* highlighting the neighborhood of the loading point. (Scale bars, 2 cm.) (*G*) Force–displacement curves for loads applied at edges A and B.

with the previous case, both the naked-eye inspection of the edge deformations in Fig. 4*F* and the force–displacement histories in Fig. 4*G* suggest that the two edges behave almost identically, i.e., the lattice is not polarized. To appreciate the entire loading process, see Movie S4.

Nonreciprocal Response of Square-Rhombus "Folded Kirigami". Next, we characterize the mechanical behavior of the square-rhombus "folded kirigami" whose fabrication by folding is described in Fig. 3*D*. This configuration was one of two systems discussed by Coulais et al. (37) in a work aimed at demonstrating

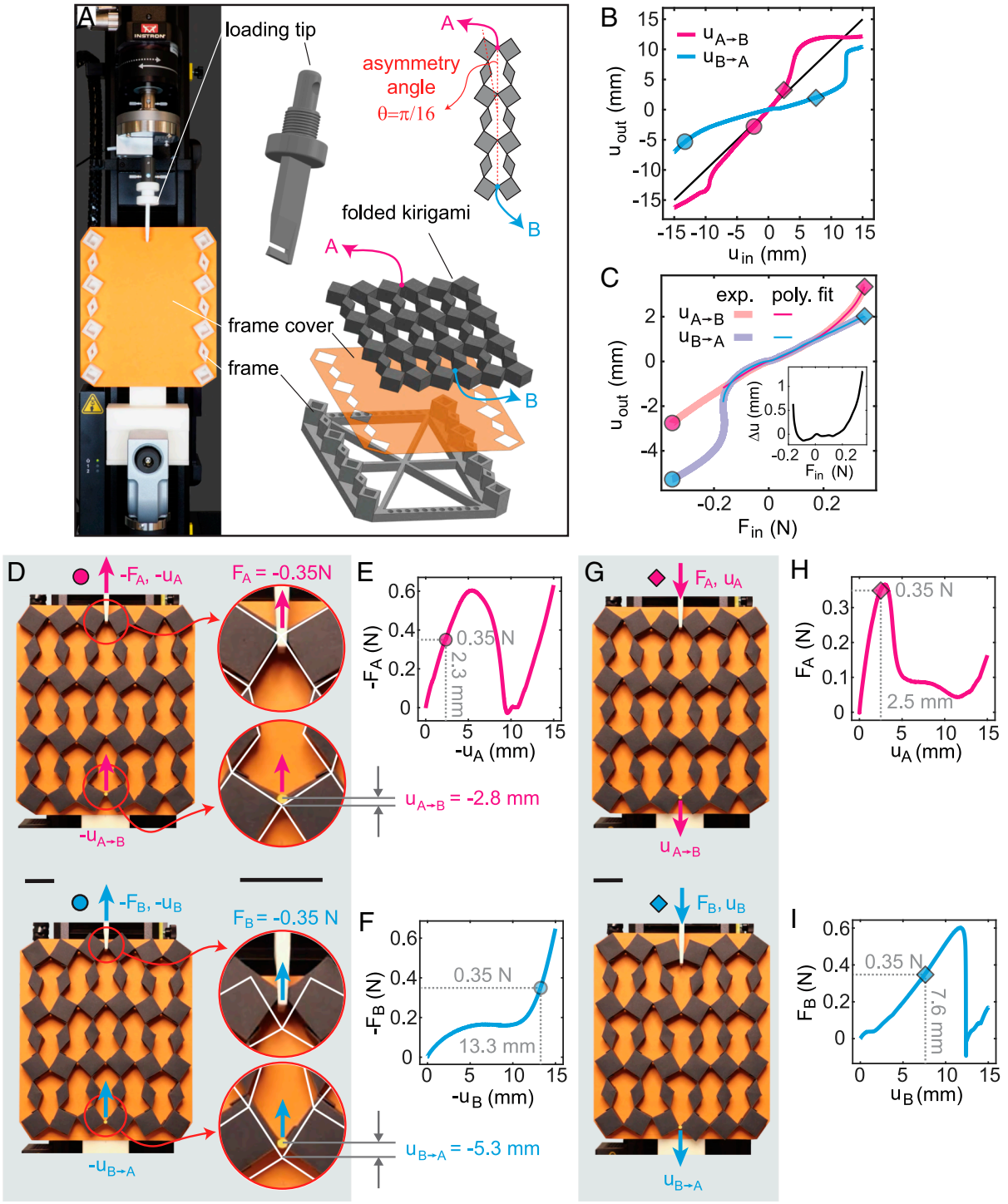

Fig. 5. Experimental validation of nonreciprocity of square-rhombus "folded kirigami". (*A*) Setup for the compression and tension tests. (*B*) Experimental curves of output displacement u_{out} versus input displacement u_{in} for loads applied at points A (magenta) and B (blue). (*C*) Experimental curves (and polynomial fit) of output displacement u_{out} versus input force F_{in} loaded at points A and B, revealing nonreciprocal behavior for large deformations. *Inset*: Nonreciprocal measurement $\Delta u = u_{A\to B} - u_{B\to A}$, obtained by plotting the difference of the two polynomials. (*D*) Snapshots showing lattice deformations for tensile loads applied at points A (magenta) and B (blue). (Scale bars, 3 cm.) (*E* and *F*) Force–displacement curves for tensile loads. (*G*) Snapshots showing lattice deformations for compressive loads applied at points A (magenta) and B (blue). (Scale bars, 3 cm.) (*H* and *I*) Force–displacement curves for compressive loads.

the realization of static nonreciprocity in mechanical systems. The kirigami pattern consists of alternating squares and rhombi, relatively twisted as shown in Fig. 5*A*. A key feature of the pattern is that, if we consider a two-quad-wide strip of lattice, the squares meet at a vertex, while the rhombi are isolated, as shown in the *Top Right* of Fig. 5*A*, making the lattice globally undercoordinated and capable of supporting floppy modes in the bulk. In ref. 37, the purpose of this configuration was to emulate, in a realistic setting, the behavior of an ideal chain of quadrilateral elements connected by rods, for which theoretical analysis predicted a topologically protected nonreciprocal response. Here, the rhombi were to play the role of the rods, while maintaining

structural integrity through their ability to be compressed without buckling.

The peculiar behavior described in ref. 37, which we intend to replicate in our "folded kirigami", was elicited in a displacement-control test by exerting quasi-statically a (tensile or compressive) input displacement u_{in} on a point on a selected edge, and by measuring the corresponding input force F_{in} on this point and the output displacement u_{out} experienced by a corresponding point on the opposite edge, de facto extracting a measure of "static transmissibility." It was found that, under proper loads that induce a regime of finite deformation, the system displays a nonreciprocal response, characterized by a highly asymmetrical edge response with u_{out} under the same F_{in} varying dramatically depending on the selected input edge and diverging as the imposed displacement becomes more nonlinear. Fig. 5*A* shows the experimental setup designed ad hoc to establish these loading conditions to the "folded kirigami". Again, the prototype is secured to a support frame that constrains selected boundary cells (in our case, the two external columns). The load is applied through an especially designed tip endowed with an anchor to engage a hinge located between a pair of square cells on the loaded edge (*SI Appendix*, Fig. S4*C*).

The results for tensile loads applied to edge A and B are given in Fig. 5*D* (with force–displacement histories shown in *E* and *F*), and in Fig. 5*G* (with force–displacement histories shown in *H* and *I*) for compressive loads. Comparing the snapshots in Fig. 5*D*, it is easy to appreciate by naked eyes that a load (here 0.35 N, measured by the load cell) applied at A causes a small displacement at B, while the same load applied at B causes a displacement at A that is nearly double (5.3 mm versus 2.8 mm). This dichotomy is captured in Fig. 5*B*, where we plot u_{out} versus u_{in} for an input displacement prescribed at A and an output displacement measured at B ($u_{A\to B}$, magenta curve), and for an input displacement prescribed at B and an output displacement measured at A ($u_{B\to A}$, blue curve), aggregating tensile conditions ($u_{in} < 0$), and compressive conditions ($u_{in} > 0$) in the same plot. The curves reproduce remarkably well the trend measured in ref. 37 on a silicone rubber specimen made by casting and curing. Specifically, the conspicuous differences between the $u_{A\to B}$ and $u_{B\to A}$ curves highlight the asymmetry between the edges.

The most telling result is the one in Fig. 5*C*, which shows the measured force–displacement relations for loads applied at A and B, color-coded as described above. This plot captures the emergence of nonreciprocal behavior in the nonlinear regime. For sufficiently large tensile or compressive loads (here approximately $|F_{in}| > 0.2$ N), the curves diverge, implying that the displacement measured at B due to a force applied at A differs from the displacement measured at A due to a force of the same magnitude applied at B. In contrast, the fact that the curves coalesce in the $|F_{in}| < 0.2$ N range confirms that, in the small deformation regime where linear elasticity can be reasonably assumed, the behavior is reciprocal, consistent with the Maxwell-Betti theorem. To appreciate the entire loading process, see Movie S5.

Discussion

We have proposed the concept of "folded kirigami" and a systematic approach to designing the crease-slit patterns required to realize a variety of configurations. The crease-slit patterns are generated by extending convex polygons with wings and (truncated) flaps, and inherit the high genus from the original kirigami patterns. The thickness dimension is lifted by folding up the wings and flaps, creating hinges and featuring a balance between flexibility from low in-plane stiffness and structural integrity from moderate out-of-plane stiffness and strength. As illustrated in *SI Appendix*, Fig. S5, the 3D printed rotating squares with soft hinges can hardly resist bending deformation. On the other hand, the stiff hinges cause large rotational stiffness that hinders reconfiguration functionality. In contrast, the "folded kirigami" possesses superior flexibility at the folds, especially the extremely low rotational stiffness near the neutral state, while maintaining out-of-plane stiffness and strength.

We have demonstrated the versatility of the "folded kirigami" against a diverse array of classical and advanced kirigami patterns—regular kagome pattern, rotating-square pattern, irregular kagome pattern, and square-rhombus pattern. In the folding process, most area of the high-genus surface is consumed to form the side walls of the "folded kirigami", causing an area shrinkage from the initial surface regarding the projecting area of the final stereoscopic structure. For the classical and advanced "folded kirigami" mentioned above, the area shrinkage is generally over 80%, as reported in *SI Appendix*, Table S1.

We have fabricated paper models and conduct mechanical testing to verify a repertoire of metamaterial functionalities, including reconfigurability, transformability between polarization and nonpolarization, and nonreciprocity. Experimental results show that the "folded kirigami" perform on par with metamaterials fabricated by conventional methods. We thus envision that this work will open a path for achieving mechanical metamaterials through the potential of surface cutting and folding, bypassing the conventional requirements of additive or subtractive manufacturing, by means of the "folded kirigami" approach.

Materials and Methods

Fabrication. We fabricated all the physical models by perforating creases and cuts on craft paper (Canson Colorline, 150 g/m^2 to 92lb) through laser engraving and cutting (Universal Laser Systems, PLS6.150D). The flaps were attached to the prisms with superglue (Loctite Ultra Gel Control) for the regular kagome "folded kirigami" in Fig. 1*D* and rotating-square "folded kirigami" in *SI Appendix*, Fig. S3*D*, and with double-sided tapes (3M 8153LE-300LSE) for the irregular kagome "folded kirigami" in Fig. 2*D* and the square-rhombus "folded kirigami" in Fig. 3*D*. The regular kagome "folded kirigami" in Fig. 1*D* has equilateral base triangles of side lengths 30 mm and thickness 17.3 mm. The rotating-square "folded kirigami" in *SI Appendix*, Fig. S3*D* has base squares of side lengths 30 mm and thickness 30 mm. The irregular kagome "folded kirigami" in Fig. 2*D* has equilateral base triangles of side lengths 20 mm, and irregular base triangles of side lengths 14.4 mm, 20 mm, and 11.4 mm; the thickness $h = 11.5$ mm and flap residual side length $s = 9.5$ mm. The square-rhombus "folded kirigami" in Fig. 3*D* has base squares of diagonal lengths 30mm, and base rhombi of diagonal lengths 30 mm and 15 mm; the thickness $h = 15$ mm and flap residual side length $s = 7.5$ mm. In Figs. 4 and 5, we fabricated the frames and fixtures by 3D printing (Ultimaker S3 and S7) with Polylactic Acid; we fabricated the loading tips by 3D printing (Stratasys J55 Prime) with Vero photopolymers; we fabricated the frame covers by laser cutting (Universal Laser Systems, PLS6.150D) craft paper (Canson Colorline, 150 g/m^2 to 92lb).

Simulation. Movies S1 and S3 were generated by performing *Motion Study* in the commercial software Solidworks (2024). The Movie S2 was generated by coding formulations in *SI Appendix*, section 2 and visualizing the patterns in the commercial software Matlab (R2023b).

Mechanical Tests and Data Processing. The quasi-static compression and tension tests in Figs. 4 and 5 were performed on the Instron materials testing

machine (Model 68SC-05 Single Column Table Mode) at the loading rate of 5 mm/min (displacement control). The force was measured by the Instron static load cell (2530-5N). The homemade experimental appliances are shown in *SI Appendix*, Fig. S4. The output displacements in Fig. 5 *B* and *C* were obtained by tracking the yellow dot (Fig. 5 *D* and *G*) in original video recordings of the testing, with the function *vision.PointTracker* in the Computer Vision Toolbox in Matlab (R2023b). The polynomial curve fitting in Fig. 5*C* was done with the function *polyfit* in the commercial software Matlab (R2023b). We pursued overfitting with polynomials of degree 50.

Data, Materials, and Software Availability. All study data are included in the article and/or supporting information.

ACKNOWLEDGMENTS. We thank Dr. Shixi Zang for helping with the mechanical testing. G.H.P. and X.D. acknowledge partial support from the Margareta E. Augustine Professorship of Engineering at Princeton University and the NSF (CMMI-2323276). S.G. acknowledges support from the NSF (CMMI-2027000).

Author affiliations: [a]Department of Civil and Environmental Engineering, Princeton University, Princeton, NJ 08544; [b]Department of Civil, Environmental, and Geo- Engineering, University of Minnesota, Minneapolis, MN 55455; and [c]Princeton Materials Institute, Princeton University, Princeton, NJ 08544

Author contributions: X.D., S.G., and G.H.P. designed research; X.D. and S.G. performed research; X.D. contributed new reagents/analytic tools; X.D., S.G., and G.H.P. analyzed data; and X.D., S.G., and G.H.P. wrote the paper.

1. K. Bertoldi, V. Vitelli, J. Christensen, M. Van Hecke, Flexible mechanical metamaterials. *Nat. Rev. Mater.* **2**, 1–11 (2017).
2. P. Jiao, J. Mueller, J. R. Raney, X. Zheng, A. H. Alavi, Mechanical metamaterials and beyond. *Nat. Commun.* **14**, 6004 (2023).
3. R. Lakes, Foam structures with a negative Poisson's ratio. *Science* **235**, 1038–1040 (1987).
4. S. Babaee *et al*., 3D soft metamaterials with negative Poisson's ratio. *Adv. Mat.* **25**, 5044–5049 (2013).
5. Y. Ding, Z. Liu, C. Qiu, J. Shi, Metamaterial with simultaneously negative bulk modulus and mass density. *Phys. Rev. Lett.* **99**, 093904 (2007).
6. H. Huang, C. Sun, G. Huang, On the negative effective mass density in acoustic metamaterials. *Int. J. Eng. Sci.* **47**, 610–617 (2009).
7. R. Zhu, X. Liu, G. Hu, C. Sun, G. Huang, Negative refraction of elastic waves at the deep-subwavelength scale in a single-phase metamaterial. *Nat. Commun.* **5**, 5510 (2014).
8. J. Shim, C. Perdigou, E. Chen, K. Bertoldi, P. Reis, Buckling-induced encapsulation of structured elastic shells under pressure. *Proc. Natl. Acad. Sci. U.S.A.* **109**, 5978–5983 (2012).
9. A. Rafsanjani, K. Bertoldi, Buckling-induced kirigami. *Phys. Rev. Lett.* **118**, 084301 (2017).
10. C. L. Kane, T. C. Lubensky, Topological boundary modes in isostatic lattices. *Nat. Phys.* **10**, 39–45 (2014).
11. J. Paulose, B. G. G. Chen, V. Vitelli, Topological modes bound to dislocations in mechanical metamaterials. *Nat. Phys.* **11**, 153–156 (2015).
12. D. Z. Rocklin, Directional mechanical response in the bulk of topological metamaterials. *New J. Phys.* **19**, 065004 (2017).
13. X. Mao, T. C. Lubensky, Maxwell lattices and topological mechanics. *Annu. Rev. Condens. Matter Phys.* **9**, 413–433 (2018).
14. G. Baardink, A. Souslov, J. Paulose, V. Vitelli, Localizing softness and stress along loops in 3D topological metamaterials. *Proc. Natl. Acad. Sci. U.S.A.* **115**, 489–494 (2018).
15. D. Zhou, L. Zhang, X. Mao, Topological edge floppy modes in disordered fiber networks. *Phys. Rev. Lett.* **120**, 068003 (2018).
16. H. Kedia, A. Souslov, D. Z. Rocklin, Soft topological modes protected by symmetry in rigid mechanical metamaterials. *Phys. Rev. B* **103**, L060104 (2021).
17. K. Sun, A. Souslov, X. Mao, T. Lubensky, Surface phonons, elastic response, and conformal invariance in twisted kagome lattices. *Proc. Natl. Acad. Sci. U.S.A.* **109**, 12369–12374 (2012).
18. O. R. Bilal, R. Süsstrunk, C. Daraio, S. D. Huber, Intrinsically polar elastic metamaterials. *Adv. Mat.* **29**, 1700540 (2017).
19. M. Pishvar, R. L. Harne, Soft topological metamaterials with pronounced polar elasticity in mechanical and dynamic behaviors. *Phys. Rev. Appl.* **14**, 044034 (2020).
20. J. N. Chapuis, T. S. Lumpe, K. Shea, Mechanical properties of topological metamaterials. *Extreme Mech. Lett.* **55**, 101835 (2022).
21. C. Widstrand, C. Hu, X. Mao, J. Labuz, S. Gonella, Stress focusing and damage protection in topological maxwell metamaterials. *Int. J. Solids Struct.* **274**, 112268 (2023).
22. M. Guzman, X. Guo, C. Coulais, D. Carpentier, D. Bartolo, Model-free characterization of topological edge and corner states in mechanical networks. *Proc. Natl. Acad. Sci. U.S.A.* **121**, e2305287121 (2024).
23. W. Zunker, S. Gonella, Soft topological lattice wheels. *Extreme Mech. Lett.* **46**, 101344 (2021).
24. J. C. Jolly *et al*., Soft mechanical metamaterials with transformable topology protected by stress caching. *Adv. Sci.* **10**, 2302475 (2023).
25. C. Widstrand, X. Mao, S. Gonella, Robustness of stress focusing in soft lattices under topology-switching deformation. *Extreme Mech. Lett.* **68**, 102135 (2024).
26. J. Tao, H. Khosravi, V. Deshpande, S. Li, Engineering by cuts: How kirigami principle enables unique mechanical properties and functionalities. *Adv. Sci.* **10**, 2204733 (2023).
27. A. Rafsanjani, L. Jin, B. Deng, K. Bertoldi, Propagation of pop ups in kirigami shells. *Proc. Natl. Acad. Sci. U.S.A.* **116**, 8200–8205 (2019).
28. X. Dang, F. Feng, H. Duan, J. Wang, Theorem on the compatibility of spherical kirigami tessellations. *Phys. Rev. Lett.* **128**, 035501 (2022).
29. G. P. Choi, L. H. Dudte, L. Mahadevan, Programming shape using kirigami tessellations. *Nat. Mater.* **18**, 999–1004 (2019).
30. X. Dang, F. Feng, H. Duan, J. Wang, Theorem for the design of deployable kirigami tessellations with different topologies. *Phys. Rev. E* **104**, 055006 (2021).
31. M. A. Dias *et al*., Kirigami actuators. *Soft Matter* **13**, 9087–9092 (2017).
32. Y. Hong *et al*., Boundary curvature guided programmable shape-morphing kirigami sheets. *Nat. Commun.* **13**, 530 (2022).
33. G. P. T. Choi, L. H. Dudte, L. Mahadevan, Compact reconfigurable kirigami. *Phys. Rev. Res.* **3**, 043030 (2021).
34. L. H. Dudte, G. P. Choi, K. P. Becker, L. Mahadevan, An additive framework for kirigami design. *Nat. Comput. Sci.* **3**, 443–454 (2023).
35. L. Wu, D. Pasini, Zero modes activation to reconcile floppiness, rigidity, and multistability into an all-in-one class of reprogrammable metamaterials. *Nat. Commun.* **15**, 3087 (2024).
36. D. Z. Rocklin, S. Zhou, K. Sun, X. Mao, Transformable topological mechanical metamaterials. *Nat. Commun.* **8**, 14201 (2017).
37. C. Coulais, D. Sounas, A. Alu, Static non-reciprocity in mechanical metamaterials. *Nature* **542**, 461–464 (2017).
38. S. Guest, J. Hutchinson, On the determinacy of repetitive structures. *J. Mech. Phys. Solids* **51**, 383–391 (2003).
39. J. Ma, D. Zhou, K. Sun, X. Mao, S. Gonella, Edge modes and asymmetric wave transport in topological lattices: Experimental characterization at finite frequencies. *Phys. Rev. Lett.* **121**, 094301 (2018).
40. L. Iorio, R. Ardito, S. Gonella, Edge-selective reconfiguration in polarized lattices with magnet-enabled bistability. *Extreme Mech. Lett.* **71**, 102217 (2024).